Sena-Cruz, J.; Branco, J.; Jorge, M.; Barros, J.A.O.; Silva, C.; Cunha, V.M.C.F. (2011) "Bond behavior between glulam and GFRP's by pullout tests." Composites Part B: Engineering. (DOI:10.1016/j.compositesb.2011.10.022)

BOND BEHAVIOR BETWEEN GLULAM AND GFRP'S BY PULLOUT TESTS

José Sena-Cruz [a], Jorge Branco [b], Marco Jorge [c], Joaquim A.O. Barros [d], Catarina Silva [e], Vitor Cunha [f]

[a] Assistant Professor, ISISE, Univ. of Minho, Dept. of Civil Engineering, Campus de Azurém, 4810-058 Guimarães, Portugal.
Tel. +351 253 510 200; Fax: +351 253 510 217
E-mail: jsena@civil.uminho.pt; ***Corresponding author***

[b] Assistant Professor, ISISE, Univ. of Minho, Dept. of Civil Engineering
E-mail: jbranco@civil.uminho.pt

[c] Researcher, ISISE, Univ. of Minho, Dept. of Civil Engineering
E-mail: marco@civil.uminho.pt

[d] Associate Professor, ISISE, Univ. of Minho, Dept. of Civil Engineering
E-mail: barros@civil.uminho.pt

[e] PhD student, ISISE, Univ. of Minho, Dept. of Civil Engineering
Email: catarina.vilaca.silva@gmail.com

[f] Assistant Professor, ISISE, Dept. of Engineering, School of Science and Technology, University of Trás-os-Montes e Alto Douro, 5001-801 Vila Real, Portugal.
E-mail: vcunha@utad.pt

Abstract: To evaluate the bond behavior between glulam and GFRP rods, applied according to the near-surface mounted strengthening technique, an experimental program composed of beam and direct pullout tests was carried. In this experimental program three main variables were analyzed: the GFRP type, the GFRP location into the groove, and the bond length. From the monitoring system it was registered the loaded and free end slips, and the pullout force. Based on these experimental results, and applying an analytical-numerical strategy, the local bond stress-slip relationship was calculated. In this work the tests are described, the obtained results are presented and discussed, and the applicability of the inverse analysis to obtain the local bond law is demonstrated.

Keywords: A. Glass fibres; A. Wood; B. Bonding; C. Numerical analysis.

1. INTRODUCTION

Glued laminated (glulam) timbers appeared for the first time at the beginning of the XX century, by Otto Hetzer. Since then, glued laminated technology faced great improvements. Nowadays, the manufacturing process of glulam is strict and industrialized, which makes the geometry very precise, the moisture content can be controlled, and mechanical properties can be obtained with relatively low dispersion. This leads to the possibility of developing glulam of higher mechanical resistance and elasticity modulus when comparing to solid wood. Glulam materials have widely been used in transportation infrastructures (e.g. bridges), and in roofs of pavilions.

In the last two decades, considerable research has been done with fiber reinforced polymer (FRP) materials for the repair or strengthening of existing structures. High stiffness and tensile strength, low weight, easy installation procedures, high durability (no corrosion), electromagnetic permeability and practically unlimited availability in terms of geometry and size are the main advantages of these composites. Despite of these main advantages, some key issues like durability and long-term performance of FRP materials still deserve a great effort of research (ACI 2008 [1]).

Currently, the most common strengthening techniques using FRP systems are (ACI 2008 [1]): the externally bonded reinforcement (EBR) and the near-surface mounted (NSM). The EBR strengthening technique has been widely studied and used, not only in concrete structures, but also in timber structures. The NSM technique is more recent, but its effectiveness in the flexural and shear strengthening is quite relevant. When compared to EBR, the NSM reinforcement has some advantages, such as (De Lorenzis and Teng 2007 [2]): (a) the amount of *in situ* installation work may be reduced, as surface preparation other than grooving is no longer required (e.g., covering removal is not necessary; irregularities of the timber surface can be more easily accommodated); (b) NSM reinforcement is less prone to debond from the substrate; (c) NSM elements can be more easily anchored into adjacent members to prevent debond failures; (d) NSM elements are protected by the wood cover and so are less exposed to accidental impact and mechanical damage, fire, and vandalism; (e) the aesthetic of the strengthened structure is virtually unchanged.

In the literature few publications can be found related to the applications of FRP's with the NSM technique to timber structures, e.g. Borri *et al.* (2005) [3], Johnsson *et al.* (2006) [4], Ahmad (2010) [5].

The results pointed out in these research works revealed good performance of the NSM technique to increase both the load carrying capacity and the stiffness.

In the context of any strengthening technique, bond behavior is an important issue, since it governs the performance of the composite strengthening system. The bond performance influences not only the ultimate load-carrying capacity of a reinforced element but also some serviceability aspects, such as deformation and crack width (this last one for the concrete structures). In the last decades several test methods have been proposed and used within the bond research scope, mainly in concrete material. The most common are the direct and the beam pullout tests. At the present time, there is no general agreement about the correct test setup to assess the bond behavior for the distinct FRP systems (Barros and Costa 2010 [6]).

To study the bond behavior between glulam and GFRP rods, applied according to the NSM strengthening technique, an experimental program composed of direct and beam pullout tests was carried out. The influence of GFRP type, the FRP location into the groove and the bond length, on the bond behavior was investigated. In the following sections the tests are described in detail, and the obtained results are presented and discussed. Using these results and applying an inverse analysis procedure, the local bond stress-slip relationship is derived.

2. EXPERIMENTAL PROGRAM

2.1 Specimens and Test Configuration

The experimental program was composed of sixty six validated pullout bond tests. Bond lengths ranging between 30 and 180 mm were adopted in order to assess its influence on the bond behavior. The lower bond length value, 30 mm, was considered since the bond length must be large enough to be representative of the glulam-FRP's interface conditions and to make negligible the unavoidable end effects. The upper bound was limited to 180 mm due to limitations associated to the specimen's geometry.

The code names given to the test series consist on alphanumeric characters separated by underscores (see Table 1). The first string indicates the GFRP type (GFRP1 and GFRP2). The second string defines the groove's depth at which the FRP was installed (D1 and D2). Finally, the last string indicates the bond length in millimeters (for instance, Lb30 represents a specimen with a bond length of

30 mm). Fig. 1(a) shows the specimen geometry and the configuration of direct pullout tests (DPT). The specimen consists of a glulam block of $140 \times 200 \times 400$ mm^3 dimensions, in which a FRP is embedded. The bond test region was located in the upper part of the block, and several bond lengths, L_b, were analyzed (30, 60 and 120 mm for the D1 series; 30, 60, 120 and 180 mm for D2 series). To avoid a premature splitting failure in the glulam ahead the loaded end, the bond length started 50 mm far from the block end. The instrumentation of the specimens consisted on three linear variable differential transducers (LVDT) and a load cell. The LVDT1 was used to control the test, at 2 μm/s slip rate, and to measure the slip at the loaded end, s_l, while the displacement transducer LVDT2 was used to measure the slip at the free end, s_f. The LVDT3 was used to measure the rotation of the specimen. The applied force, F, was registered by a load cell placed between the specimen top surface and the actuator. The overall layout of the performed tests is depicted in Fig. 1(b).

Fig. 2(a) shows the specimen geometry and configuration adopted for the beam pullout tests (BPT). The specimen is composed by two glulam blocks (block A and B) of equal dimensions, $140 \times 200 \times 300$ mm^3, interconnected by a steel hinge located at mid-span in the top part, and also by the FRP fixed at the bottom in which the FRP is embedded. The bond test region was located in the bottom part of block A, and several bond lengths, L_b, were analyzed (see Table 1). Like in the DPT, to avoid premature splitting failure in the glulam ahead the loaded end, the bond length started 50 mm far from the block end. The instrumentation of these specimens consisted on two LVDT's, a strain gauge and a load cell. The LVDT2 was used to control the test, at 2 μm/s slip rate, and to measure the slip at the loaded end, s_l, while the LVDT1 was used to measure the slip at the free end, s_f. The applied force, F, was transmitted to the specimen through a steel plate that, in turn, transmits $F/2$ through two steel rods to the glulam blocks. The applied force was registered by a load cell placed between the steel plate and the actuator. A strain gauge, placed at the mid-span of the specimen, measured the FRP strains during the test (applied in one specimen per each series).

2.2 Material characterization

2.2.1 Timber

In the present experimental program glued laminated timber, currently named by glulam, of strength class GL24h (NP EN 1194:1999 [7]), was used for all the series. The material characterization of the GL24h

included compression and tension tests parallel to the grain, according to EN 408 [8]. Sixteen specimens were used for each type of test. From the compression tests, an average compressive strength of 27.99 MPa with a coefficient of variation (CoV) of 17.6%, and an average modulus of elasticity of 6.62 GPa (CoV=27.8%) were obtained. From the tension tests, an average tensile strength, a modulus of elasticity and a strain at the peak stress of 55.93 MPa (CoV=16.7%), 9.17 GPa (CoV=11.9%) and 6.35‰ (CoV=12.4%) were obtained, respectively.

2.2.2 GFRP rod

The GFRP rod used in the present work, with a trademark Maperod G, was provided in rolls of 6 meters each, and was supplied by MAPEI®. Two distinct types of Maperod G are available on the market. According to the supplier the major difference is limited to the external surface of these rods (see Fig. 3). In the present work both rods were studied and hereinafter, the rod with a rougher external surface will be denominated as GFRP2, whereas the other as GFRP1. These rods have a nominal diameter of 10 mm and the external surface is sand blasted.

Tensile tests were carried out to assess the tensile mechanical properties of each GFRP rod type, according to ISO TC 71/SC 6 N - Part 1 - (2003) [9]. Tests were performed under a displacement rate of 2 mm/min. To measure the modulus of elasticity, a clip gauge was mounted at middle region of each specimen. The results obtained from the mechanical characterization of the GFRP rods are presented in Table 2. In this table F_{fmax} is the maximum force, whereas σ_{fmax} is the corresponding tensile strength; $\sigma_{fmax}= F_{fmax}/A_f$; A_f is the GFRP cross-sectional area evaluated with the nominal diameter of the rod; E_f is the longitudinal elasticity modulus evaluated according the aforementioned standard; the strain at the maximum stress ε_{fmax} was evaluated assuming linear behaviour up to peak stress. Both GFRP rods have similar response, not only in terms of tensile strength but also in terms of modulus of elasticity. Nevertheless, GFRP2 presents a modulus of elasticity slightly higher. Very low values of the coefficients of variation (CoV) were obtained for the case of GFRP1, but a rather high value of CoV was registered for the strain at the maximum tensile stress for the GFRP2. For all the specimens the failure mode was explosive due to the fiber progressive rupture.

2.2.3 Epoxy adhesive

In the present experimental work the epoxy MapeWood Paste 140, supplied by MAPEI®, was used. This thixotropic epoxy adhesive is currently used for the restoration of timber structural elements, and is composed of two premeasured parts (Part A = resin and Part B = hardener). To assess the mechanical properties of the hardened adhesive, tensile tests were carried out according to ISO 527-2 (1993) [10]. After casted, the six specimens were kept in the laboratory environment in the vicinity of the pullout specimens, and they were tested at the same age of the pullout tests. The adhesive specimens were tested in a universal test machine, at a displacement rate of 1 mm/min. A clip gauge mounted on the middle zone of the specimen recorded the strains, whereas a high accurate load cell has registered the applied force. From the tests an average tensile strength of 17.15 MPa (CoV=7.5%), modulus of elasticity of 8.11 GPa (CoV=17.6%) and a strain at peak stress of 0.26% (CoV=19.6%) were obtained.

2.3 Preparation of Specimens

The preparation of the strengthened specimens required several steps. The NSM strengthening procedures are quite well documented in the literature (De Lorenzis and Teng 2007 [2]; Barros *et al.* 2007 [11]) and specific detailed information related to the specimens used in the present work can be found elsewhere (Jorge 2010 [12]). After strengthening, the specimens were kept in the laboratory environment before being tested. The pullout tests were carried out at least 10 days after the application of the FRP reinforcement.

3. RESULTS AND DISCUSSION

Fig. 4 depicts the average pullout force *versus* loaded end slip (F_l-s_l) relationships for all the tested series, whereas Tables 3 and 4 include the main results obtained on the direct and beam pullout tests (DPT and BPT), respectively. In these tables F_{fmax} is the maximum pullout force; F_{fu} is FRP tensile strength (see also Table 2); $\tau_{max,av1}$ and $\tau_{max,av2}$ are the average bond stress at the rod-epoxy and glulam-epoxy interfaces, respectively, and are evaluated by $F_{fmax} / (P_f L_b)$ and $F_{fmax} / (P_g L_b)$, where P_f is the perimeter of the FRP cross-section and P_g is perimeter of the groove cross-section in contact with the adhesive; s_{fmax} and s_{lmax} are the free end and loaded end slips at F_{fmax}, respectively.

The pullout force was directly evaluated by the values registered in the load cell for the case of direct pullout configuration. In the beam pullout tests, two distinct approaches were initially adopted (see Fig. 2): (i) the first one was based on the force values measured at the load cell and takes into account the internal lever arm, i.e., the distance between the longitudinal axis of the GFRP and the contact point at the steel hinge; (ii) the second approach is based on the values recorded by the strain gage glued to the GFRP rod and takes into account the corresponding modulus of elasticity and its cross sectional area. In general no significant differences were found between both approaches (Jorge 2010 [12]); so, in the context of the present work the first one was adopted.

In the direct pullout tests the records registered by the LVDT1 (see Fig. 1) include not only the loaded end slip, s_l, but also the elastic deformation of the FRP between the loaded end section and the top surface of the timber block (50 mm of distance). In the present analysis only the s_l was considered.

In general, the F_l-s_l responses are characterized by a short linear branch followed by a nonlinear response up to peak load. In some series post-peak response can be observed. When the type of test is compared, beam pullout tests yielded to superior performance, not only in terms of higher peak load, but also a more ductile response, since the F_l-s_l responses always include a post-peak phase. In the pullout bending tests the FRP bar is simultaneously submitted to an axial force and a curvature due to the rotation of the beam. The influence of the curvature is higher at the loaded end vicinity. The relative vertical displacement between the top surface of the groove and the top surface of the bar introduces a lateral confinement pressure in the bar. Assuming that the behaviour of the GFRP-glulam interface system can be governed by a Mohr-Coulomb model, this lateral pressure increases the bond resistance, which is responsible for the higher peak bond force registered in the BPT.

From these figures is also visible that the peak pullout force and the slip at this load level increase with the bond length. Furthermore, comparing Fig. 4(a-b) with (c-d) it can be concluded that the rougher external surface of the GFRP2 rod contributed to increase the peak pullout force and the corresponding loaded end slip (see also Tables 3 and 4), since similar mechanical properties were obtained in the experimental characterization of these bars (see Table 2). The increase in terms of F_{fmax} due to the distinct surface treatment of the GFRP rods, found for the series Lb30, Lb60 and Lb120 was 16%, 35% and 29% and, 7%, 11% and 25% for the DPT and BPT, respectively. From this statement is evident fact the effect of the influence of the external surface was more important for the case of DPT.

Fig. 4(e-f) shows that the benefits in terms of peak pullout force derived from installing the GFRP bar into the groove as deeper as possible was only relevant for the larger bond lengths (120 and 180 mm). From the comparison of the D1 and D2 curves it can be concluded that the pullout capacity increases with the depth that the bar is installed into the groove, which is in agreement with results obtained with NSM CFRP laminates (Costa and Barros 2011 [13]).

Analyzing the results included in Tables 3 and 4 the following main conclusions can be pointed out:

- The F_{fmax} increases with the bond length. The maximum average value occurred for the GFRP1_D2_Lb180 of the BPT series, i.e. in the series with a GFRP deeper placed into the groove;
- As expected, the pullout efficiency, defined by the F_{fmax} / F_{fu} ratio, increased with the bond length. For the case of the BPT an average of about 80% was attained in the GFRP1_D2_Lb180;
- As expected, bond strength has decreased with the increase of the bond length (see columns of $\tau_{max,av1}$ and $\tau_{max,av2}$) due to the non-constant tangential stress along the longitudinal axis of the FRP (Sena-Cruz and Barros 2004 [14]). It was also predictable higher values for $\tau_{max,av1}$ when compared with $\tau_{max,av2}$, since the contact area for the latter is larger;
- In general, all the parameters present quite low values of the corresponding coefficients of variation. The exception is for the values of slips at the loaded and free ends. In fact high coefficients of variation were observed, and an eventual justification can be attributed to the difficulty in measuring this physical entity;
- Fig. 5 shows the principal obtained failure modes: (i) glulam shear failure (GS); (ii) glulam/adhesive interfacial sliding (GAI); (iii) FRP/adhesive interfacial sliding and adhesive splitting (FAI+SPL). Analyzing the failure modes obtained no special tendency can be observed.

Fig. 6 presents the influence of the bond length (L_b) on the following parameters: pullout force efficiency (F_{max}/F_{fu}), loaded end slip (s_l), average bond strength at FRP/adhesive interface (τ_{av1}), and average bond strength at adhesive/glulam interface (τ_{av2}). The F_{max}/F_{fu} ratio and the s_l have increased with

the bond length, however, a non-asymptotic trend can be observed. Larger L_b values need to be investigated to obtain the maximum values for the F_{max}/F_{fu} ratio. The increase rate of s_l with L_b seems to increase linearly with L_b. A distinct trend is observed for the series GFRP1_D2. Fig. 6 also evidences the benefits in terms of F_{max}/F_{fu} and τ_{av1}, when the rod is deeper installed into the groove. The better performance that can be achieved when selecting a bar of rougher surface is quite visible in terms of F_{max}/F_{fu} and bond stresses. The decrease of the average bond stress with the increment of the bond length in all tested series seems to tend to an asymptotic value.

4. NUMERICAL ANALYSIS

The mathematical representation of the pullout phenomenon is often expressed by a second order differential equation, which can be established either in terms of forces (Naaman *et al.* 1990 [15], Sujvorakul *et al.* 2000 [16], Banholzer *et al.* 2005 [17]), or derived in terms of slip (Russo *et al.* 1990 [18], Focacci *et al.* 2000 [19], Sena-Cruz and Barros 2004 [14]). In the present work the local bond law was established in terms of slip and obtained by an inverse analysis procedure. Here, it will be presented a brief overview of the analytical formulation. The detailed description of the analytical model, as well as the inverse analysis strategy can be found elsewhere (Sena-Cruz and Barros 2004 [14], Sena-Cruz *et al.* 2006 [20]). The adopted analytical model to obtain the local bond stress–slip law has shown a good predictive performance on modeling a diversity of pullout test results, such as: near-surface mounted CFRP laminate strips (Sena-Cruz *et al.* 2006 [20]), galvanized steel rebar (Sena-Cruz *et al.* 2009 [21]), discrete steel fibers embedded in concrete medium (Cunha *et al.* 2008 [22], 2010 [23]).

4.1 Local bond-slip

The equilibrium of the free body with an infinitesimal length *dx* of a GFRP rod bonded to glulam by an adhesive can be given by:

$$\sigma_f \cdot A_f + \tau \cdot P_f \cdot dx = \left(\sigma_f + d\sigma_f\right) \cdot A_f \tag{1}$$

where $\tau = \tau[s(x)]$ is the local bond shear stress acting on the contact surface between the rod and the glulam, and *s* is the slip, i.e. the relative displacement between the GFRP and the glulam. Finally, σ_f, A_f and P_f are the normal stress, cross section area and perimeter of the GFRP rod, respectively.

Assuming that the GFRP has a linear elastic constitutive law in the longitudinal direction ($d\sigma_f = E_f \cdot d\varepsilon_f$) and neglecting the glulam deformability in the slip determination, after simplification of Eq. 1, the second order differential equation that governs the local bond phenomena of the bar-matrix interface is given by:

$$\frac{d^2 s}{dx^2} = \frac{P_f}{E_f A_f} \cdot \tau(x) \tag{2}$$

4.2 Pullout load-slip relationship

Consider a GFRP rod inserted in glulam over a bond length L_b, where N is the generic applied pullout force, and s_f and s_l are, respectively, the free and loaded end slips (see Fig. 7). When the GFRP rod is slipping due to an applied pullout force, $\bar{N}$, the following functions can be evaluated along the rod bond length: slip along the rod, $s(x)$; bond shear stress along the embedded length, $\tau(x)$; GFRP strain, ε_f; and the axial force, $N(x)$, where the origin of x axis coincides with the free extremity of the bond length.

In Fig. 7 the slip diagram along the rod, $s(x)$, can be regarded as the sum of two components. A constant component, s_f, which produces a rigid body displacement of the GFRP, whereas the $s_d(x)$ component results from the deformation of the GFRP. Moreover, for any point x of the GFRP embedded length, just the $s_d(x)$ component will result in a GFRP rod length change, thus the rod deformation at a point x is obtained from $\varepsilon_f(x) = N(x)/(E_f A_f)$. The pullout force is given by Eq. 3, which was obtained by equating both the internal and external work produced, respectively, by the rod elastic deformation and the bond stress profile at the GFRP interface (Sena-Cruz *et al.* 2009 [21]).

$$N = \sqrt{2E_f \cdot A_f \cdot P_f \cdot \int_{s_f}^{s(x=\tilde{L}_b)} \tau(s) \cdot ds} \tag{3}$$

The analytical bond stress-slip relationship used in the present work is defined by Eq. 4, where τ_m and s_m are, respectively, the bond strength and its corresponding slip. Parameter α defines the shape of the pre-peak branch, whereas α' determines the shape of the post-peak branch.

$$\tau(s) = \tau_m \left(\frac{s}{s_m}\right)^{\alpha}, s \le s_m \wedge \tau(s) = \tau_m \left(\frac{s}{s_m}\right)^{-\alpha'}, s > s_m \tag{4}$$

4.3 Numerical procedure

Considering the entities described in Fig. 7, the boundary conditions at the free and loaded ends are indicated in Eq. 5. Numerical and experimental entities are simultaneously used; hence the experimental one was distinguished by an overline, i.e. $\overline{N}^i$ represents for the pullout force experimentally measured in the *i-th* experimental scan read-out.

$$x = 0 \rightarrow \begin{cases} s(0) = s_f \\ N(0) = 0 \\ \varepsilon_f(0) = 0 \end{cases} \quad \wedge \quad x = L_b \rightarrow \begin{cases} s(L_b) = s_l \\ N(L_b) = \overline{N} \\ \varepsilon_f(L_b) = N(L_b) / \left(E_f A_f \right) \end{cases} \tag{5}$$

The GFRP rod pullout tests provide data in terms of pullout force, $\overline{N}$, and free-end slip, $\bar{s}_f$, for several scan read-outs, being $\bar{s}_f^i$ and $\overline{N}^i$ the values of the *i-th* scan read out. Regarding these experimental results, the set of unknown parameters of the local bond relationship (τ_m, s_m, α, α' comprised in Eq. 4) is desired to be found in order to fit the differential Eq. 2 as accurately as possible. Further details of the developed algorithm to obtain the local bond law by inverse analysis can be found elsewhere (Sena-Cruz *et al*. 2004 [14], 2006 [20]).

4.4 Numerical results

The local bond stress-slip relationship for each series was calibrated from the average experimental pullout load-slip curve. In this study was primarily intended to model the pullout behavior up to the maximum load. On the inverse analysis process, the search of α and α' of the local bond relationship was conducted within the interval]0, 1], whereas for τ_m and s_m no boundaries were fixed. For the longitudinal elasticity modulus, the average values obtained on the mechanical characterization of the GFRP rods were used (see Table 2). For the geometrical properties, a cross-sectional area, A_f, of 78.54 mm^2 and a cross-sectional perimeter, P_f, of 31.415 mm were adopted.

The pullout force *vs.* loaded end slip (F_l-s_l) curves obtained by the numerical inverse analysis procedure and experimentally, are compared in Fig. 8, being possible to conclude that the developed numerical strategy can predict with good accuracy the (F_l-s_l) curves. The parameters of the local bond law defined in Eq. 4, which lead to the numerical (F_l-s_l) curves, are included in Tables 5 and 6 for the bending and direct pullout tests, respectively. Moreover, in Tables 5 and 6, is also included the normalized error, *Err*, of the numerical fitting process to the experimental curve defined by the ratio between *e* and the area

under the experimental curve, being *e* the area between the experimental and numerical curves; the ratio between the maximum experimental pullout load and the maximum numerical pullout, F_{fmax}/F_{fnum}; and the ratio between the loaded end slip at F_{fmax} and the loaded end slip at F_{fnum}, s_{fmax}/s_{fnum}. In general, the obtained *Err* was relatively small with the exception of GFRP1_D2_Lb60 series that exceeded 10%. The F_{fmax}/F_{fnum} ratio obtained is close to the unit, [0.985-1.059], which shows the good accuracy on the estimation of the maximum pullout load. On the other hand, for s_{fmax}/s_{fnum} the F_{fmax}/F_{fnum} ratio ranged from 0.949 to 1.129, with several series with values close to the unit.

Analyzing the parameters of the local bond stress law obtained by inverse analysis, included in Tables 5 and 6, the following main conclusions can be pointed out:

- In general, the slip at maximum bond stress, s_m, increases with the bond length, for both the beam and direct pullout tests;
- The maximum bond stress, τ_m, decreases with the increase of the bond length, for both the beam and direct pullout series. GFRP1_D2_Lb60 series for both beam and direct tests are exceptions. Moreover, higher values of τ_m were obtained for the bending pullout test configuration;
- For α parameter, which defines the shape of the pre-peak branch, it was not visualized any clear trend with the variation of the bond length. Nevertheless, the values of α obtained from the simulation of direct pullout tests where rather higher than the ones obtained from the beam pullout tests. An average value of 0.88 was obtained for the direct tests, whereas for the beam tests an average value of 0.57 was obtained. Notice that the allowed interval for parameter α ranges from 0 to 1.0. Moreover, as α tends to 1.0, the concavity of the pre-peak branch diminishes tending to a straight segment;
- No clear trend was observed for α'. This was expected since α' controls the shape of the post-peak branch bond law, which has more preponderance on the softening phase of the pullout load – slip response. However, notice that α' also influences the pullout load–slip response up to the maximum load. In Fig. 9 is depicted an example of the local bond stress τ variation over the GFRP longitudinal embedded length (x) corresponding to the maximum pullout load. It can be observed, for the maximum pullout load, that at the loaded end (x = 60 mm) the local bond strength, τ_m, was already attained for a lower pullout force.

Fig. 10 depicts the bond length influence on the numerical average bond strength, $\tau_{av,num}$, and on numerical bond strength, τ_m. The values of $\tau_{av,num}$, which are included in Tables 5 and 6, were computed in a distinct fashion from the average bond strength $\tau_{max,av1}$ and $\tau_{max,av2}$ obtained from the experimental results. The procedure to calculate $\tau_{av,num}$ was the following: *i)* for each series, at the maximum pullout load was obtained the corresponding slip variation over the longitudinal embedded length, $s(x)$; *ii)* the bond stress variation along the embedded length, $\tau(x) = \tau[s(x)]$, is determined adopting for the local bond law the parameters obtained from the inverse analysis; *iii)* the area under $\tau(x)$ is computed; *iv)* finally $\tau_{av,num}$ is obtained by dividing the area under $\tau(x)$ diagram by the corresponding embedment length, L_b. In Fig. 9 is also depicted $\tau_{av,num}$ obtained for the beam series GFRP1_D2_Lb60. The computed values of $\tau_{av,num}$, as expected, were smaller than the τ_m. Moreover, in general, they were within the envelope of the average bond strength values at the FRP/adhesive interface, $\tau_{max,av1}$, see Fig. 10a.

5. CONCLUSIONS

The present work presented an experimental study on bond characterization between GFRP rods and glulam, using the near surface mounted (NSM) strengthening technique, through beam and direct pullout tests (BPT and DPT). The type of GFRP rod (GFRP1 and GFRP2), the groove geometry/FRP location (D1 and D2) and the bond length (L_b=30, 60, 120 and 180 mm) were the main variables studied.

The maximum pullout force (F_{fmax}), the loaded and free ends slips (s_l and s_f), and the ratio between maximum pullout force and the FRP strength (F_{fmax} / F_{fu}) have increased with L_b, while the bond strength (τ_{max}) has decreased with the increase of L_b. A rougher external surface of the rod (GFRP2) has provided a better bond performance, as well as a deeper installation of the GFRP into the groove (D2). In general, the pullout force *versus* loaded end slip relationships (F_l-s_l) are characterized by a short linear branch followed by a nonlinear response up to peak load. When the type of test is compared, BPT yielded to superior performance, not only in terms of peak load, but also in the ductility of the F_l-s_l response.

Failure modes included glulam shear failure, interfacial failure glulam/adhesive, interfacial failure FRP/adhesive and adhesive splitting.

Using a numerical approach, a local bond stress-slip relationship was obtained from the test results. The parameters that define this relationship were, however, found to be dependent on the bond length.

ACKNOWLEDGEMENTS

This work is supported by FEDER funds through the Operational Programme for Competitiveness Factors - COMPETE and National Funds through FCT – Portuguese Foundation for Science and Technology under the project PTDC/ECM/74337/2006. The authors also like to thank all the companies that have been involved supporting and contributing for the development of this study, mainly: INEGI, S&P Clever Reinforcement Ibérica Lda., Portilame, MAPEI and Rothoblaas.

REFERENCES

1. ACI 440.2R-08. Guide for the Design and Construction of Externally Bonded FRP Systems for Strengthening Concrete Structures. Reported by ACI Committee 440, American Concrete Institute, 2008, 80 pp.

2. De Lorenzis L, Teng JG. Near-surface mounted FRP reinforcement: An emerging technique for strengthening structures. Composites Part B 2007, 38(2):119-143.

3. Borri A, Corradi M, Grazini A. A method for flexural reinforcement of old wood beams with CFRP materials. Composites: Part B 2005, 36, 143–153.

4. Johnsson H, Blanksvärd T, Carolin A. Glulam members strengthened by carbon fibre reinforcement. Materials and Structures 2006, 40, 47–56.

5. Ahmad Y. Bending behavior of timber beams strengthened using fiber reinforced polymer bars and plates. PhD Dissertation, Faculty of Civil Engineering, Technology University of Malaysia, 2010, 306 pp.

6. Barros JAO, Costa IG. Bond Tests on Near Surface Reinforcement Strengthening for Concrete Structures. EN-CORE/fib Round Robin Testing Initiative, Report no. 09/DEC/E-30 Department of Civil Engineering, University of Minho, 2010.

7. NP EN 1194:1999. Timber structures. Glulam wood. Strength classes and determination of the chacateristic values. Instituto Português da Qualidade, Lisbon, 2009. (in Portuguese)

8. EN 408. Timber structures - Structural timber and glued laminated timber. Determination of some physical and mechanical properties. European Committee for Standardization (CEN), 2003, 31 pp.

9. ISO TC 71/SC 6 N Part 1. Non-conventional reinforcement of concrete-test methods: Fiber reinforced polymer (FRP) bars. International Organization for Standardization (CEN), 2003, 48 pp.

10. ISO 527-2. Plastics - Determination of tensile properties - Part 2: Test conditions for molding and extrusion plastics. International Organization for Standardization (CEN), 1993.

11. Barros JAO, Dias SJE, Lima JLT. Efficacy of CFRP-based techniques for the flexural and shear strengthening of concrete beams. Cement and Concrete Composites 2007, 29(3):203-217.

12. Jorge MAP. Experimental behavior of glulam-FRP systems. MSc thesis, Department of Civil Engineering, University of Minho, 2010, 247 pp.

13. Costa IG, Barros, JAO. Assessment of the bond behavior of NSM FRP materials by pullout tests. In: Proceedings of in First Middle East Conference on Smart Monitoring, Assessment and Rehabilitation of Civil Structures, Dubai, 2011.

14. Sena-Cruz JM, Barros JAO. Modeling of bond between near-surface mounted CFRP laminate strips and concrete. Computers and Structures Journal 2004, 82:1513-1521.

15. Naaman AE, Namur GG, Alwan JM, Najm HS. Fiber pullout and bond slip I: Analytical study. Structural Engineering 1990, 117(9):2769-2790.

16. Sujivorakul C, Waas AM, Naaman A. Pullout response of a smooth fiber with an end anchorage. Engineering Mechanics 2000, 126(9):986-993.

17. Banholzer B, Brameshuber W, Jung W. Analytical simulation of pull-out tests – the direct problem. Cement & Concrete Composites 2005, 27:93-101.

18. Russo G, Zingone G, Romano F. Analytical solution for bond-slip of reinforcing bars in R.C. joints. Structural Engineering 1990, 116(2):336-355.

19. Focacci F, Nanni A, Bakis C. Local bond-slip relationship for FRP reinforcement in concrete. Composites for Construction 2000, 4(1):24-31.

20. Sena-Cruz JM, Barros JAO, Gettu R, Azevedo AFM. Bond behavior of near-surface mounted CFRP laminate strips under monotonic and cyclic loading. Composites for Construrction 2006, 10(4):295-303.

21. Sena-Cruz JM, Cunha VMCF, Camões A, Barros JAO, Cruz P. Modeling of bond between galvanized steel rebars and concrete. In: Proceedings of Congreso de Métodos Numéricos en Ingeniería, CIMNE, Barcelona, Spain, 2009, 15 pp.

22. Cunha, V.M.C.F., Barros J.A.O., Sena-Cruz J.M. (2008) Bond-slip mechanisms of hooked-end steel fibres in self-compacting concrete, Materials Science Forum, 587-588:877-881.

23. Cunha, V.M.C.F., Sena-Cruz, J.M., Barros, J. A. O. (2010) "Pullout Behavior of Steel Fibers in Self-Compacting Concrete" ASCE Journal Materials in Civil Engineering, 22(1):1-9.

TABLE CAPTIONS

Table 1 – Experimental program

Table 2 – Main results obtained on the mechanical characterization of the GFRP rods (average values)

Table 3 – Main results obtained on the direct pullout tests, DPT (average values)

Table 4 – Main results obtained on the beam pullout tests, BPT (average values)

Table 5 – Local bond stress–slip relationship parameters obtained from IA of the pullout bending tests

Table 6 – Local bond stress–slip relationship parameters obtained from IA of the direct pullout tests

Table 1 – Experimental program

Material	**Depth** (mm)	L_b (mm)	**Denomination**	**N. of specimens**
GFRP1	15	30	GFRP1_D1_Lb30	6 (D); 4 (B)
		60	GFRP1_D1_Lb60	6 (D); 2 (B)
		120	GFRP1_D1_Lb120	6 (D); 4 (B)
GFRP1	20	30	GFRP1_D2_Lb30	2 (D); 3 (B)
		60	GFRP1_D2_Lb60	2 (D); 3 (B)
		120	GFRP1_D2_Lb120	3 (D); 3 (B)
		180	GFRP1_D2_Lb180	2 (D); 2 (B)
GFRP2	15	30	GFRP2_D1_Lb30	3 (D); 2 (B)
		60	GFRP2_D1_Lb60	3 (D); 4 (B)
		120	GFRP2_D1_Lb120	4 (D); 2 (B)

Note: D – Direct pullout test; B – Beam pullout test

Table 2 – Main results obtained on the mechanical characterization of the GFRP rods (average values)

GFRP	F_{fmax} (kN)	σ_{fmax} (MPa)	E_f (GPa)	ε_{fmax} (‰)	***Failure mode***
GFRP1	61.12 (3.5%)	778.14 (3.5%)	38.42 (1.3%)	20.25 (2.3%)	XGM (all)
GFRP2	61.15 (1.6%)	786.04 (2.8%)	41.60 (7.8%)	18.99 (10.2%)	OGM (all)

Notes: XGM – Explosive failure in gauge measuring length; OGM – Explosive failure located outside of the gauge measuring length. The values between parentheses are the corresponding coefficients of variation.

Table 3 – Main results obtained on the direct pullout tests, DPT (average values)

Series	F_{fmax} (kN)	F_{fmax} / F_{fu} (%)	$\tau_{max,av1}$ (MPa)	$\tau_{max,av2}$ (MPa)	s_{fmax} (mm)	s_{lmax} (mm)	*Failure mode*
GFRP1_D1_Lb30	9.58	15.68	10.17	6.97	0.25	0.34	FAI+SPL
	(5.6%)	(5.6%)	(5.6%)	(5.3%)	(13.2%)	(17.0%)	
GFRP1_D1_Lb60	16.89	27.64	8.96	6.13	0.31	0.62	FAI+SPL
	(11.4%)	(11.4%)	(11.4%)	(11.3%)	(22.3%)	(19.5%)	
GFRP1_D1_Lb120	24.17	39.54	6.41	4.39	0.29	0.86	FAI+SPL (5)*
	(5.0%)	(5.0%)	(5.0%)	(5.3%)	(5.5%)	(12.9%)	FAI+GS+SPL (1)*
GFRP1_D2_Lb30	11.10	17.98	11.78	6.65	0.12	0.21	GAI+FAI; GAI
	(4.5%)	(4.5%)	(4.5%)	(4.6%)	(2.7%)	(23.1%)	
GFRP1_D2_Lb60	22.83	36.98	12.11	6.79	0.22	0.44	FAI+CR; GS
	(0.9%)	(0.9%)	(0.9%)	(0.9%)	(24.2%)	(22.8%)	
GFRP1_D2_Lb120	31.29	50.69	8.30	4.67	0.20	1.02	GAI; GAI+FAI;
	(4.2%)	(4.2%)	(4.2%)	(4.6%)	(20.6%)	(12.4%)	GAI+GS
GFRP1_D2_Lb180	37.78	61.20	6.68	3.76	0.15	1.30	GS; FAI
	(8.9%)	(8.9%)	(8.9%)	(9.1%)	(37.8%)	(5.7%)	
GFRP2_D1_Lb30	11.84	19.18	12.57	8.65	0.33	0.32	FAI+GAI+SPL;
	(8.8%)	(8.8%)	(8.8%)	(8.4%)	(15.0%)	(22.9%)	GAI ; FAI+SPL
GFRP2_D1_Lb60	20.17	32.67	10.70	7.30	0.36	0.66	FAI+GAI+SPL;
	(2.4%)	(2.4%)	(2.4%)	(2.3%)	(15.1%)	(8.8%)	GAI+FAI; AI+GS
GFRP2_D1_Lb120	31.44	50.93	8.34	5.75	0.35	1.01	FAI+CR (1)*
	(4.0%)	(4.0%)	(4.0%)	(4.0%)	(8.1%)	(7.0%)	FAI+SPL (3)*

Notes: FAI – FRP/adhesive interfacial sliding; GAI – glulam/adhesive interfacial sliding; SPL – adhesive splitting; GS – glulam shear failure; CR – adhesive cracking; FF – FRP failure; the percentages values between parenthesis are the corresponding coefficients of variation; *the value between parenthesis is the number of specimens with this type of failure mode.

Table 4 – Main results obtained on the beam pullout tests, BPT (average values)

Series	F_{fmax} (kN)	F_{fmax} / F_{fu} (%)	$\tau_{max,av1}$ (MPa)	$\tau_{max,av2}$ (MPa)	s_{fmax} (mm)	s_{lmax} (mm)	*Failure mode*
GFRP1_D1_Lb30	11.81	19.32	12.53	8.62	0.09	0.20	FAI+CR (3)*;
	(9.3%)	(9.3%)	(9.3%)	(10.0%)	(71.6%)	(31.0%)	GAI+FAI+CR
GFRP1_D1_Lb60	20.19	33.04	10.71	7.43	0.12	0.45	FAI+CR
	(0.2%)	(0.2%)	(0.2%)	(0.7%)	(93.8%)	(13.9%)	
GFRP1_D1_Lb120	27.42	44.87	7.31	5.00	0.06	0.90	FAI+CR
	(2.0%)	(2.0%)	(2.6%)	(2.1%)	(96.6%)	(12.1%)	
GFRP1_D2_Lb30	12.64	20.68	13.41	7.58	0.07	0.17	GAI; FAI+CR;
	(11.0%)	(11.0%)	(11.0%)	(11.5%)	(62.1%)	(28.2%)	FAI+GAI+CR
GFRP1_D2_Lb60	22.46	36.76	11.92	6.76	0.11	0.36	GAI; FAI+CR; GS
	(5.7%)	(5.7%)	(5.7%)	(5.6%)	(25.3%)	(21.0%)	
GFRP1_D2_Lb120	34.29	57.15	9.10	5.15	0.06	0.95	GAI+FAI+CR (1)*;
	(8.9%)	(8.9%)	(8.9%)	(9.1%)	(48.8%)	(3.4%)	FAI+CR (2)*
GFRP1_D2_Lb180	48.49	79.36	8.58	4.83	0.19	2.91	GAI+FAI+CR;
	(13.5%)	(13.5%)	(13.5%)	(13.7%)	(35.7%)	(14.7%)	GAI+GS
GFRP2_D1_Lb30	15.49	25.09	16.44	11.21	0.25	0.30	FAI+CR; GAI
	(6.4%)	(6.4%)	(6.4%)	(7.0%)	(68.6%)	(19.7%)	
GFRP2_D1_Lb60	24.85	40.25	13.18	9.09	0.10	0.37	FAI+CR (2); GS+GAI;
	(9.9%)	(9.9%)	(9.9%)	(10.3%)	(64.6%)	(61.7%)	FAI+GAI+CR
GFRP2_D1_Lb120	33.69	54.58	8.94	6.06	0.38	0.90	FAI+CR; GS+FAI+CR
	(6.8%)	(6.8%)	(6.8%)	(4.6%)	(92.3%)	(3.1%)	

Notes: FAI – FRP/adhesive interfacial sliding; GAI – glulam/adhesive interfacial sliding; SPL – adhesive splitting; GS – glulam shear failure; CR – adhesive cracking; FF – FRP failure; the percentages values between parenthesis are the corresponding coefficients of variation; *the value between parenthesis is the number of specimens with this type of failure mode.

Table 5 – Local bond stress–slip relationship parameters obtained from IA of the pullout bending tests

Series	s_m (mm)	τ_m (MPa)	α (-)	α' (-)	*Err.* (%)	s_{fmax} / s_{fnum} (-)	F_{fmax} / F_{fnum} (-)	$\tau_{av,num}$ (MPa)
GFRP1_D1_Lb30	0.12	12.7	0.86	0.40	2.6	1.174	1.019	11.93
GFRP1_D1_Lb60	0.22	11.0	0.55	0.20	4.1	1.219	1.017	10.39
GFRP1_D1_Lb120	0.30	7.8	0.40	0.35	4.0	1.129	1.028	6.80
GFRP1_D2_Lb30	0.14	12.4	0.51	0.30	3.6	1.018	1.014	11.88
GFRP1_D2_Lb60	0.22	13.2	0.46	0.20	1.7	1.082	1.018	10.08
GFRP1_D2_Lb120	0.34	10.1	0.83	0.10	2.7	1.072	1.043	9.18
GFRP1_D2_Lb180	2.10	9.2	0.30	0.20	3.2	0.976	1.059	8.78
GFRP2_D1_Lb30	0.22	16.0	0.65	0.60	1.5	1.019	1.014	15.14
GFRP2_D1_Lb60	0.19	13.5	0.50	0.50	6.3	1.082	1.018	11.85
GFRP2_D1_Lb120	0.25	10.9	0.67	0.52	2.1	1.085	1.043	8.43

Table 6 – Local bond stress–slip relationship parameters obtained from IA of the direct pullout tests

Series	s_m (mm)	τ_m (MPa)	α (-)	α' (-)	*Err.* (%)	s_{fmax}/s_{fnum} (-)	F_{fmax}/F_{fnum} (-)	$\tau_{av,num}$ (MPa)
GFRP1_D1_Lb30	0.28	9.3	0.95	0.10	2.6	1.047	1.000	9.00
GFRP1_D1_Lb60	0.51	8.0	0.99	0.30	3.2	0.950	0.986	7.41
GFRP1_D1_Lb120	0.57	7.2	0.87	0.10	1.3	1.000	1.008	6.21
GFRP1_D2_Lb30	0.16	11.2	0.72	0.50	2.2	1.190	0.985	10.71
GFRP1_D2_Lb60	0.29	12.5	1.00	0.90	10.7	0.975	1.035	10.67
GFRP1_D2_Lb120	0.65	9.5	1.00	0.20	6.2	0.989	0.991	7.76
GFRP1_D2_Lb180	0.41	7.2	0.40	0.60	0.8	1.000	1.002	6.41
GFRP2_D1_Lb30	0.35	13.2	0.96	0.80	2.5	0.949	1.000	12.65
GFRP2_D1_Lb60	0.49	10.7	0.96	0.20	0.5	1.000	1.005	10.01
GFRP2_D1_Lb120	0.69	9.9	0.99	0.85	2.4	1.000	1.006	7.99

FIGURE CAPTIONS

Fig. 1 – Direct pullout tests: (a) Specimen geometry and configuration; (b) Layout. Note: all dimensions are in millimeters.

Fig. 2 – Beam pullout tests: (a) Specimen geometry and configuration; (b) Layout. Note: all dimensions are in millimeters.

Fig. 3 – FRP rods used in the experimental program: (a) GFRP1; (b) GFRP2.

Fig. 4 – Pullout force vs. loaded end slip for the series GFRP1_D1 (a-b), GFRP2_D1 (c-d) and GFRP1_D2 (e-f) for the beam and direct pullout tests, respectively (average curves).

Fig. 5 – Typical failure modes obtained in the pullout tests.

Fig. 6 – Bond length influence on: (a) efficiency in terms of maximum load; (b) loaded end slip; (c) average bond strength τ_{av1}; (d) average bond strength τ_{av2}.

Fig. 7 – Entities in the analytical model.

Fig. 8 – Pullout force vs. loaded end slip relationships obtained by inverse analysis for the series: GFRP1_D1 (a-b), GFRP2_D1 (c-d) and GFRP1_D2 (e-f) for the beam and direct pullout tests, respectively.

Fig. 9 – Variation of the bond stress, τ, and slip, s, along the GFRP longitudinal embedded length (x) for the beam series GFRP1_D2_Lb60.

Fig. 10 – Bond length influence on: (a) the numerical average bond strength $\tau_{av,num}$; (b) numerical bond strength τ_m.

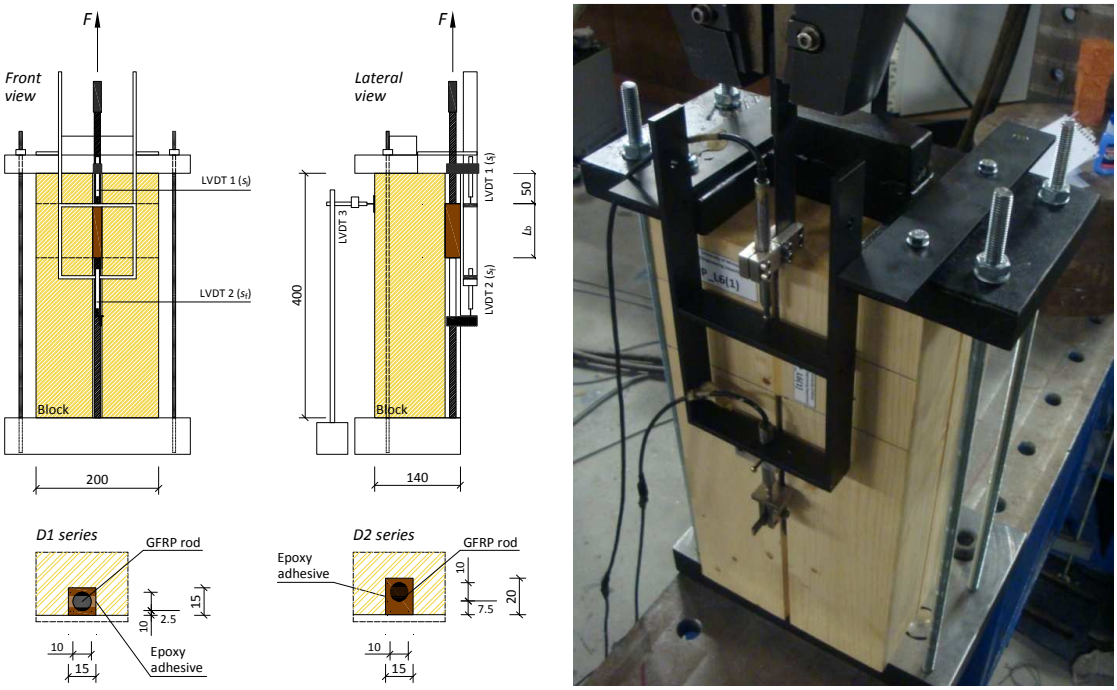

(a) (b)

Fig. 1: Direct pullout tests: (a) Specimen geometry and configuration; (b) Layout. Note: all dimensions are in millimeters.

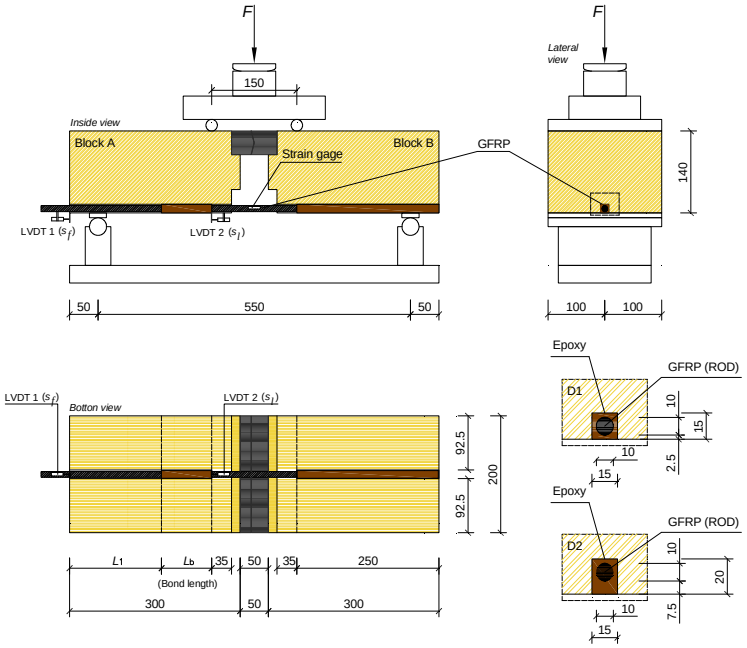

(a)

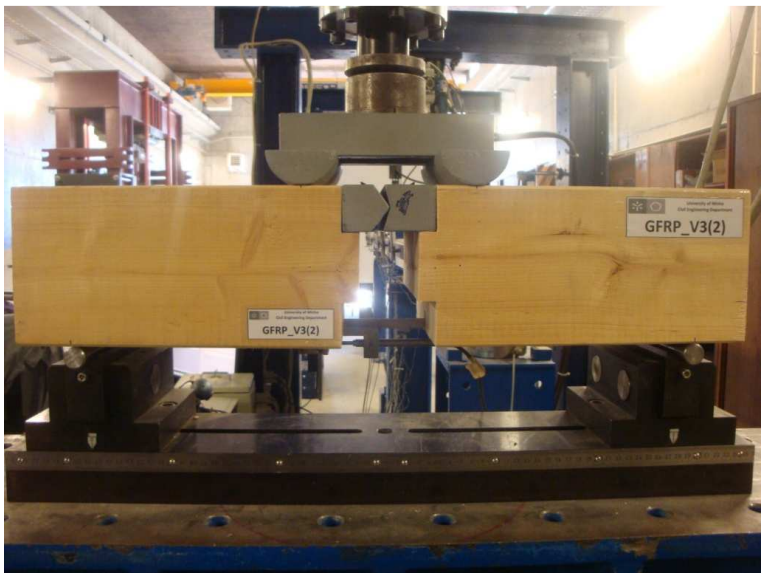

(b)

Fig. 2: Beam pullout tests: (a) Specimen geometry and configuration; (b) Layout. Note: all dimensions are in millimeters.

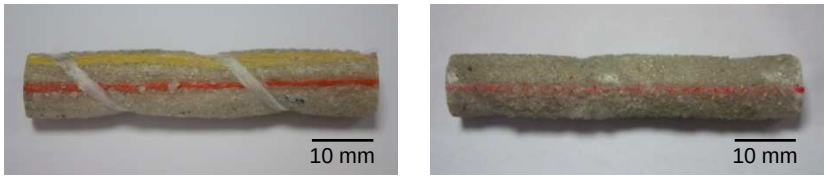

(a) (b)

Fig. 3 – FRP rods used in the experimental program: (a) GFRP1; (b) GFRP2.

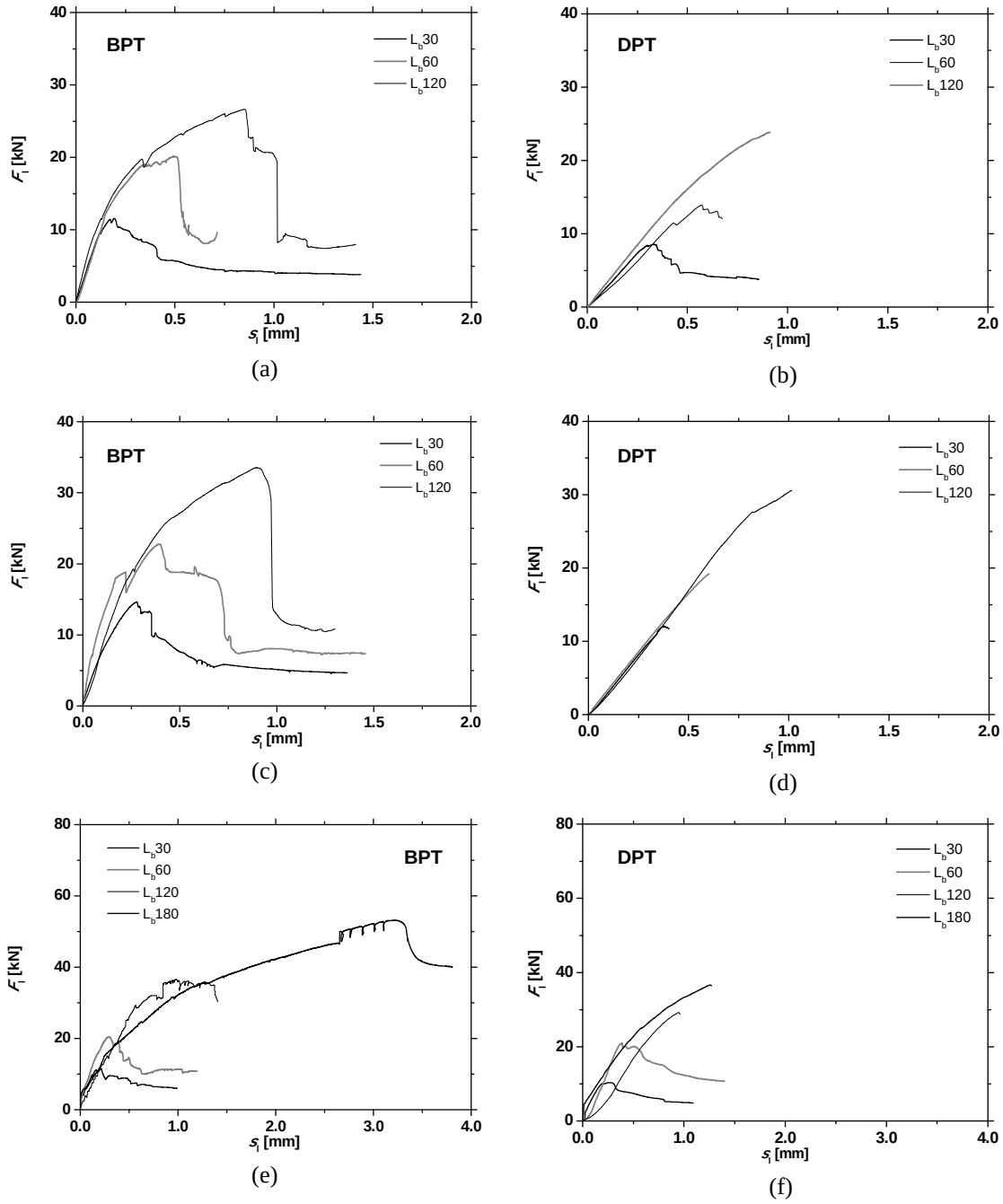

Fig. 4 – Pullout force *vs*. loaded end slip for the series GFRP1_D1 (a-b), GFRP2_D1 (c-d) and GFRP1_D2 (e-f) for the beam and direct pullout tests, respectively (average curves).

GS – Glulam shear failure

GAI – Glulam/adhesive interfacial sliding

FAI+SPL – FRP/adhesive interfacial sliding + adhesive splitting

Fig. 5 – Typical failure modes obtained in the pullout tests**.**

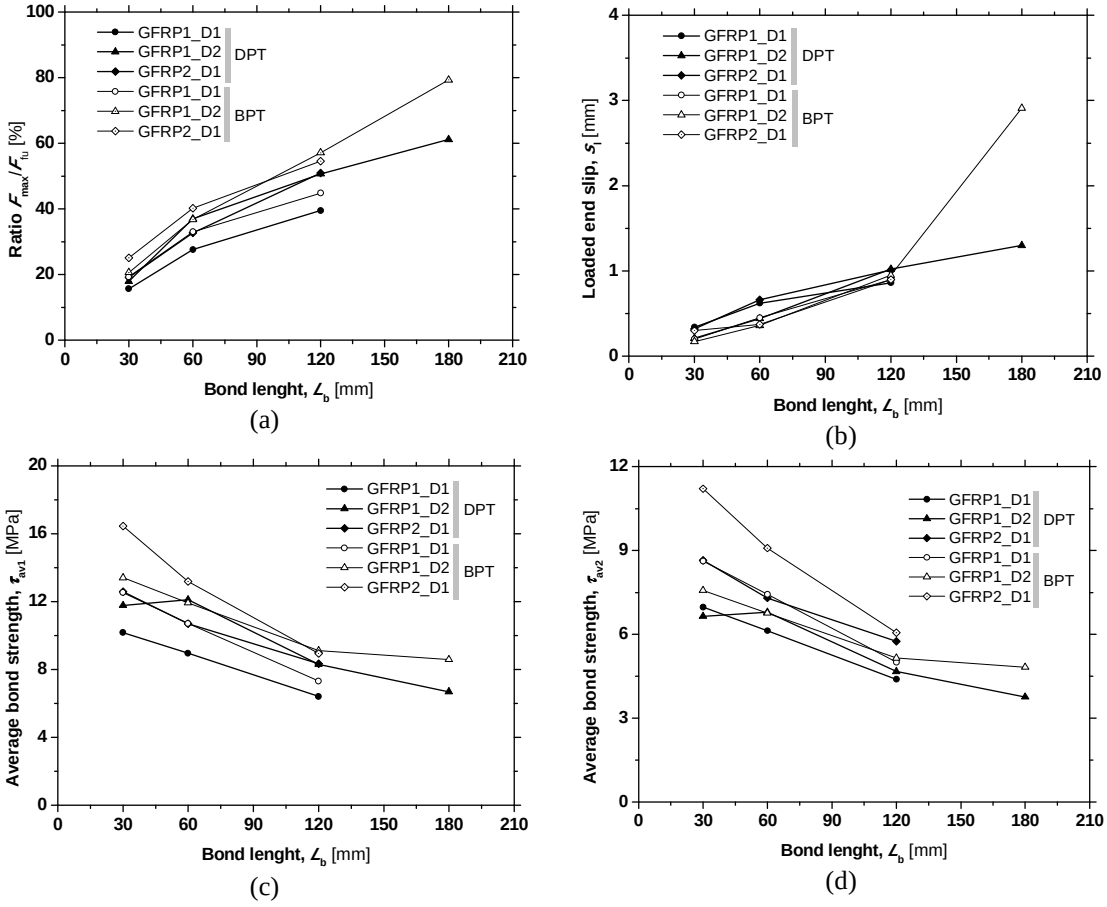

Fig. 6 – Bond length influence on: (a) efficiency in terms of maximum load; (b) loaded end slip; (c) average bond strength τ_{av1}; (d) average bond strength τ_{av2}.

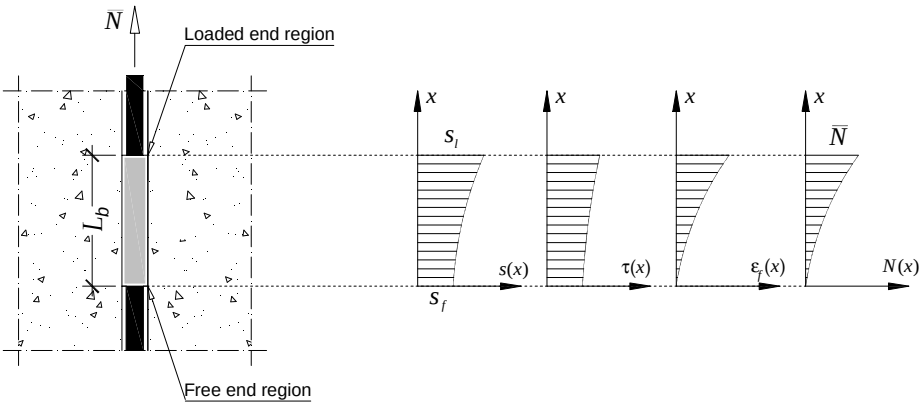

Fig. 7 – Entities in the analytical model.

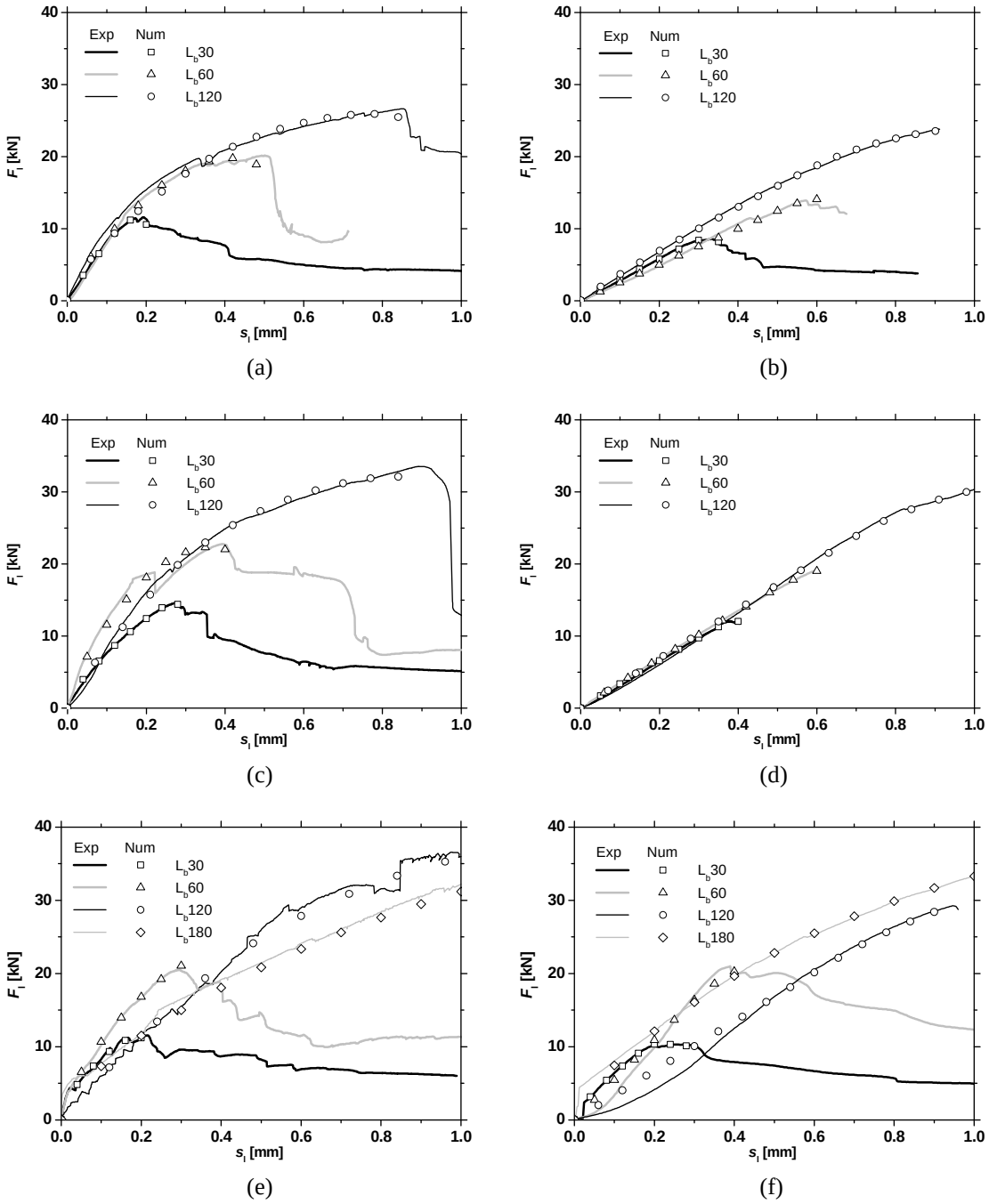

Fig. 8 – Pullout force *vs*. loaded end slip relationships obtained by inverse analysis for the series: GFRP1_D1 (a-b), GFRP2_D1 (c-d) and GFRP1_D2 (e-f) for the beam and direct pullout tests, respectively.

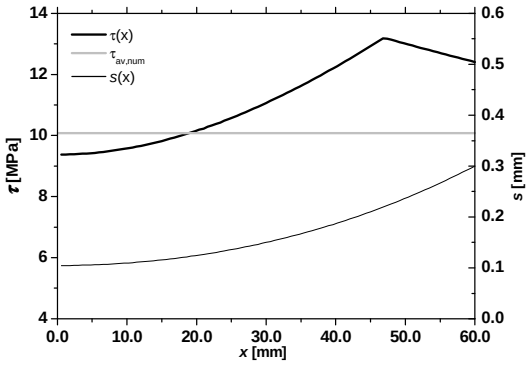

Fig. 9 – Variation of the bond stress, *τ*, and slip, *s*, along the GFRP longitudinal embedded length (*x*) for the beam series GFRP1_D2_Lb60**.**

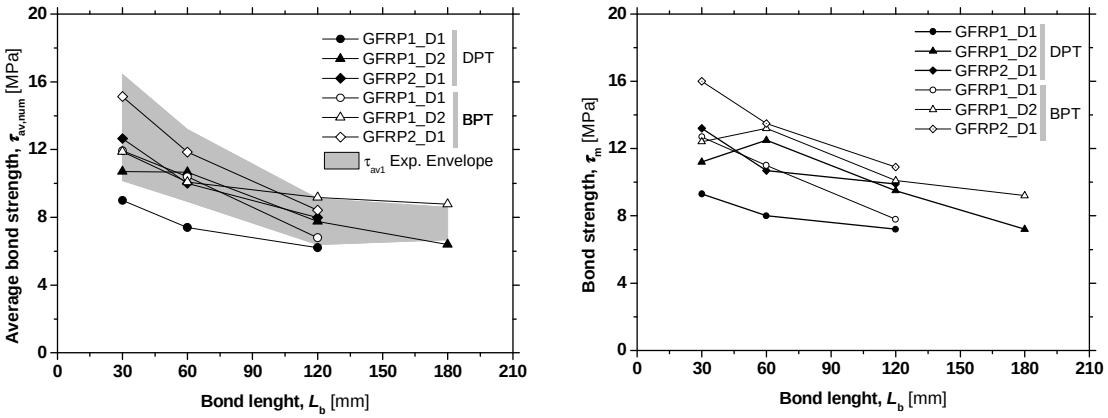

Fig. 10 – Bond length influence on: (a) the numerical average bond strength $\tau_{av,num}$; (b) numerical bond strength τ_m.